Numerical Linear Algebra with Applications

WILEY

RESEARCH ARTICLE OPEN ACCESS

An Accelerated Spectral CG-Type Projection Method With Restart Strategy for Nonlinear Monotone Equations and Applications in Compressed Sensing

Pengjie Liu[1] | Linhao Li[1] | Hu Shao[1,2] | Bowen Zhang[3]

[1]School of Mathematics, China University of Mining and Technology, Xuzhou, China | [2]Jiangsu Center for Applied Mathematics (CUMT), China University of Mining and Technology, Xuzhou, China | [3]Department of Statistics, University of Oxford, Oxford, UK

Correspondence: Hu Shao (shaohu@cumt.edu.cn)

Received: 19 August 2024 | **Revised:** 2 June 2025 | **Accepted:** 14 August 2025

Funding: This work was supported by the Fundamental Research Funds for the Central Universities (Grant No. 2025QN1147).

Keywords: compressed sensing | convergence rate | nonlinear monotone equations | restart strategy | spectral conjugate gradient projection method | theoretical convergence

ABSTRACT

In this study, we present an accelerated spectral conjugate gradient-type projection method to solve the system of nonlinear monotone equations. Compared to traditional methods for solving such equations, this method utilizes three-step successive information to produce inertial iterates. The proposed composite search direction framework incorporates an effective restart strategy, eliminating the need for additional conditions, including the specification of conjugate parameter, and satisfies conditions for the sufficient descent condition and trust region property. Establishing the theoretical convergence of the present method does not require Lipschitz continuity. Furthermore, we analyze the asymptotic and non-asymptotic convergence rates in terms of iteration complexity. To evaluate effectiveness, comparative tests are conducted against existing methods using problems related to the system of nonlinear equations. Moreover, the practicality of the presented method is demonstrated through applications in compressed sensing.

MSC2020 Classification: 65K05, 90C30, 90C56

1 | Introduction

In this study, we seek solutions to the following system of nonlinear monotone equations (referred to as SoNME):

$$\mathfrak{F}(u) = 0 \tag{1}$$

where the mapping $\mathfrak{F} : \mathbb{R}^n \to \mathbb{R}^n$ is assumed to be continuous and monotone. The monotonicity of $\mathfrak{F}$ is defined as

$$[\mathfrak{F}(u) - \mathfrak{F}(\hat{u})]^\top (u - \hat{u}) \geq 0, \quad \forall\, u,\, \hat{u} \in \mathbb{R}^n \tag{2}$$

The SoNME is a common problem that appears in various engineering applications. It is particularly relevant in fields such as economic modeling and compressive sensing, among others. A variety of iterative methods have been developed to solve the SoNME, such as derivative-based methods and derivative-free projection (DFP) methods. The latter category comprises methods such as the spectral gradient projection method [1–3] and the conjugate gradient (CG)-type projection method. These methods eliminate the need for complex computations and the storage of Jacobian matrices. Herein, we focus on the CG-type projection methods within the DFP family. These methods inherit the CG

method's advantages of streamlined iterations and minimal storage requirements.

To date, numerous iterative CG-type projection methods have been introduced to solve SoNME (1). These include two-term CG-type projection methods [4–8], spectral CG-type projection methods [9–13], and three-term CG-type projection methods [14–24], among others. For example, Ibrahim et al. [4] built upon the classical Dai-Yuan (DY) CG method and integrated the hyperplane projection approach [25] to introduce a hybrid DY-type projection method for solving the constrained SoNME (1). Without relying on the Lipschitz continuity of $\mathfrak{F}(\cdot)$, they demonstrated that the method converges globally. Abubakar et al. [10] introduced a hybrid spectral CG-type projection method for solving the constrained SoNME (1). The hybrid conjugate parameter they introduced integrates four classic conjugate parameters, including the Hestenes-Stiefel (HS), Polak-Ribière-Polyak (PRP), Fletcher-Reeves (FR), and DY parameters. Kumam et al. [11] presented another hybrid spectral CG-type method for solving the constrained SoNME (1). This method featured a convex combination of HS-type and DY-type parameters. Jiang et al. [22] initially introduced a hybrid conjugate parameter within a three-term search direction. They then employed a restart strategy, which endowed the search direction with theoretically advantageous properties.

The heavy ball method, originally introduced by Polyak [26], is a well-regarded acceleration technique that leverages momentum to enhance iterative processes. By integrating information from two consecutive iterations, this method effectively guides the next step forward. Its utility has been recognized across a variety of iterative methods, and more notably, it has been instrumental in boosting the computational efficiency of CG-type projection methods to solve nonlinear equations. Building on the three-term CG-type projection method [15] as well as the inertial technique, Ma et al. [27] proposed a modification to the CG-type projection method, specifically designed to solve constrained SoNME (1). This method incorporates an inertial extrapolation step into the search direction formulation, resulting in a direction that inherently satisfies the sufficient descent condition. Furthermore, they demonstrated the global convergence of their introduced algorithm, on the condition that the underlying mapping $\mathfrak{F}(\cdot)$ satisfies Lipschitz continuity. Employing an inertial mechanism, Wu et al. [28] introduced an inertial spectral CG-type projection method for solving constrained SoNME (1). The conjugate parameter was refined through a hybrid adaptation of the memoryless Broyden-Fletcher-Goldfarb-Shanno update. The spectral parameter, derived from the quasi-Newton formulation, was double-truncated to satisfy the sufficient descent condition. Also, Liu et al. [29] developed an inertial spectral CG-type projection method, which incorporates a parameter inspired by the method of Brazilian and Bowein to derive the spectral parameter. In addition, several studies [30–35] integrated the inertial (or inertial-relaxed) strategy into the CG projection method for solving nonlinear equations, achieving enhanced numerical performance and faster results. Recently, researchers [36, 37] incorporated an inertial strategy that utilizes three-step iterative information into the search direction and presented the corresponding inertial projection method for solving (constrained) SoNME.

Based on the aforementioned CG-type projection methods and related inertial techniques, we further develop accelerated spectral CG-type projection methods to solve SoNME (1). In this work, we construct a flexible restart direction and implement a well-defined adaptive line search. The main contributions of this work are summarized below.

1.1 | Composite Search Direction Construction

To ensure that the search direction exhibits sufficient descent, regardless of the choice of conjugate parameter, we utilize a spectral parameter to generate a CG-type search direction. Furthermore, to ensure that the proposed search direction satisfies the trust region property, we incorporate a new restart strategy. At the same time, to avoid the under-performance associated with using the negative gradient as the restart direction, we construct an effective restart direction that contains a flexible vector p_k.

1.2 | Algorithm Construction

Building upon the commonly used line search iterative forms, we suggest a new adaptive line search with a well-defined structure. Furthermore, based on the composite search direction proposed above, we incorporate a hyperplane projection approach with a relaxed step and introduce an accelerated scheme that utilizes three-step inertial information. As a result, we propose an accelerated spectral CG-type projection algorithmic framework with a restart strategy (rsASCGP-AF) to solve SoNME (1), without the need to specify a particular conjugate parameter.

1.3 | Theoretical Analysis

The composite search direction in the proposed rsASCGP-AF consistently satisfies the sufficient descent condition and trust region property, irrespective of the line search or the specific conjugate parameter. Furthermore, we establish the theoretical convergence of the rsASCGP-AF without requiring the underlying mapping $\mathfrak{F}(\cdot)$ to be Lipschitz continuous. In addition, we derive both asymptotic and non-asymptotic global convergence rates in terms of iteration complexity.

1.4 | Numerical Experiments

The proposed rsASCGP-AF is evaluated on 10 problems involving systems of nonlinear equations, demonstrating its superior performance. Furthermore, its potential applications are illustrated through experiments on compressed sensing problems.

The remaining structure is organized as follows: Section 2 presents an accelerated projection-based algorithmic framework and its associated properties. Section 3 establishes the theoretical convergence of the proposed algorithmic framework. Section 4 derives both asymptotic and non-asymptotic convergence rates in terms of iteration complexity. Section 5 presents numerical experiments and their practical applications. Finally, conclusions are provided.

2 | Motivation and Algorithmic Framework

In this study, we aim to construct a framework of spectral CG-type search directions that possess favorable theoretical properties and strong numerical performance. We then extend this framework to address the problem of solving the SoNME defined in Equation (1). However, due to the presence of various conjugate parameters, forming a robust search direction framework is challenging, as the corresponding search direction may experience stagnation during the iteration process. A common strategy to address stagnation in CG-type methods for unconstrained optimization is through "restarting", as seen in References [38–43]. This typically involves taking a step in a restart direction rather than continuing along the original search direction. The most basic approach is to restart using the steepest descent direction. Although empirical evidence suggests that this can enhance performance in practice, the method is rather simple and somewhat crude. This raises the question of whether a more effective restart direction can be identified for CG-type projection methods — one that offers better theoretical guarantees and improved numerical performance.

More recently, to address the issue of jamming in the FR-based search direction, Babaie-Kafaki et al. [44] proposed a method targeting the consecutive gradient difference vector, $y_{k-1} = \mathfrak{F}(u_k) - \mathfrak{F}(u_{k-1})$, which tends to approach zero when the sequence became jammed. Subsequently, they demonstrated a strategy to enhance the FR method and overcome jamming by leveraging the numerical benefits of using the PRP parameter as a shrinkage multiplier for the FR method. The resulting search direction is described as

$$d_k = \begin{cases} -\mathfrak{F}(u_k), & \text{if } k = 0, \\ -\left(1 + \beta_k^{\text{MIFR}} \frac{\mathfrak{F}(u_k)^\top d_{k-1}}{\|\mathfrak{F}(u_{k-1})\|^2}\right)\mathfrak{F}(u_k) + \beta_k^{\text{MIFR}} d_{k-1}, & \text{if } k \geq 1 \end{cases}$$

where the modified FR parameter β_k^{MIFR} is

$$\beta_k^{\text{MIFR}} = \min\left\{\frac{|\mathfrak{F}(u_k)^\top y_{k-1}|}{\|\mathfrak{F}(u_{k-1})\|^2},\ 1\right\} \cdot \frac{\|\mathfrak{F}(u_k)\|^2}{\|\mathfrak{F}(u_{k-1})\|^2}$$

Inspired by the construction of β_k^{MIFR}, we first define an effective restart direction as follows:

$$d_k = \begin{cases} -\mathfrak{F}(\eta_k), & \text{if } \|p_k\| = 0 \text{ or } \|y_{k-1}\| = 0, \\ -\mathfrak{F}(\eta_k) + \frac{\mathfrak{F}(u_k)^\top y_{k-1}}{\varrho \|p_k\| \cdot \|y_{k-1}\|} \cdot p_k, & \text{if } \|p_k\| \neq 0 \text{ and } \|y_{k-1}\| \neq 0, \text{ with } \varrho > 1 \end{cases} \tag{3}$$

Here, p_k is any vector, the presence of which can increase the flexibility of the restart direction.

On the other hand, generally speaking, in a CG-type projection method, finding the separating hyperplane incurs the highest computational cost. Therefore, using an appropriate line search strategy can significantly reduce the overall computational burden of this family of methods. To this end, many existing studies have exploited inexact line search strategies to obtain a well-defined step-length t_k at minimal cost, while ensuring the theoretical convergence of the algorithm. Well-known line searches that generate the separating hyperplane include:

i. Zhang and Zhou [45] applied the following line search strategy to determine the step-length t_k. They set $t_k = \max\{\varsigma\rho^i : i = 0, 1, 2, \dots\}$ such that

$$-\mathfrak{F}(u_k + t_k d_k)^\top d_k \geq \sigma t_k \|d_k\|^2 \tag{4}$$

where $\varsigma > 0$ serves as the initial estimate for the step-length, $\rho \in (0, 1)$ is a shrinkage factor, and σ is a positive constant.

ii. Li and Li [46] computed the step-length t_k as $t_k = \max\{\varsigma\rho^i : i = 0, 1, 2, \dots\}$ such that

$$-\mathfrak{F}(u_k + t_k d_k)^\top d_k \geq \sigma t_k \|\mathfrak{F}(u_k + t_k d_k)\| \|d_k\|^2 \tag{5}$$

and noted that this line search was originally proposed by Solodov and Svaiter [25].

Numerical tests have demonstrated that the line searches (4) and (5) exhibit distinct behaviors when solving problems. For instance, when u_k is far from the solution set and $\|\mathfrak{F}(u_k + t_k d_k)\|$ is excessively large, the right-hand side of (5) becomes disproportionately large. This increase leads to a rise in the computational cost of the line search and results in an excessively small step-length t_k. Conversely, a similar issue may occur with (4) when the current iterate is close to a solution and $\|d_k\|$ is unusually large. Based on these observations, it appears advantageous to employ (4) when the approximation is far from the solution set, and to switch to (5) as it nears the solution. To mitigate the aforementioned drawbacks, Amini and Kamandi [47] proposed an alternative adaptive line search strategy:

$$-\mathfrak{F}(u_k + t_k d_k)^\top d_k \geq \sigma t_k \frac{\|\mathfrak{F}(u_k + t_k d_k)\|}{1 + \|\mathfrak{F}(u_k + t_k d_k)\|} \|d_k\|^2 \tag{6}$$

which exhibits robust performance in both situations by effectively balancing its competing challenges. However, the line search in Equation (6) does not adjust for the impact of $\|d_k\|^2$, which may still lead to increased computational effort. To further address this issue, we introduce a new adaptive line search strategy that computes the step-length t_k as $t_k = \max\{\varsigma\rho^i : i = 0, 1, 2, \dots\}$ such that

$$-\mathfrak{F}(u_k + t_k d_k)^\top d_k \geq \sigma t_k \frac{\|\mathfrak{F}(u_k + t_k d_k)\|}{\mu_1 + \|\mathfrak{F}(u_k + t_k d_k)\|} \cdot \frac{\|d_k\|^2}{\mu_2 + \|d_k\|^2} \tag{7}$$

where $\varsigma > 0$, $\rho \in (0, 1)$, and $\sigma > 0$, with μ_1 (≥ 0) and μ_2 (≥ 0) being constants that ensure the adaptiveness of the line search. Given that $\frac{\|\mathfrak{F}(u_k + t_k d_k)\|}{\mu_1 + \|\mathfrak{F}(u_k + t_k d_k)\|} \in (0, 1]$ and $\frac{\|d_k\|^2}{\mu_2 + \|d_k\|^2} \in (0, 1]$, this formulation ensures that the right-hand side of (7) remains within a manageable range, thereby empirically reducing the computational burden of the line search process. Moreover, we theoretically prove that the new strategy (7) is well-defined, as shown in Lemma 2.

Next, utilizing the newly formulated restart direction (3), we derive a composite search direction incorporating an arbitrary conjugate parameter. Then, combined with the line search (7) and the accelerated scheme, we propose the rsASCGP-AF for solving SoNME. The corresponding iterative steps are outlined below.

ALGORITHM 1 | rsASCGP-AF.

Step 0. Given initial iterates $u_{-2}, u_{-1}, u_0 \in \mathbb{R}^n$. Parameters $\varepsilon > 0$, $\sigma > 0$, $\phi \in [0,1)$, $\psi \in [0,1)$, $\varrho > 1$, $c > 0$, $\varsigma > 0$, $\rho \in (0,1)$, $\mu_1 \geq 0$, $\mu_2 \geq 0$, and $0 < \underline{\gamma} \leq \gamma_k \leq \bar{\gamma} < 2$. The inertial step control sequences $\{\epsilon_k\}$ and $\{\hat{\epsilon}_k\}$, with $\epsilon_k \in [0,1)$ and $\hat{\epsilon}_k \in [0,1)$, each satisfy $\sum_{k=0}^{+\infty} \epsilon_k < +\infty$ and $\sum_{k=0}^{+\infty} \hat{\epsilon}_k < +\infty$.Let $k := 0$.

Step 1. Calculate $\mathfrak{F}(u_k)$. Terminate the process if $\|\mathfrak{F}(u_k)\| \leq \varepsilon$.

Step 2. Calculate two inertial step-lengths via

$$\phi_k = \begin{cases} \min\left\{\phi, \frac{\epsilon_k}{\|u_k - u_{k-1}\|}\right\}, & \text{if } u_k \neq u_{k-1}, \\ \phi, & \text{otherwise}, \end{cases} \quad \psi_k = \begin{cases} \min\left\{\psi, \frac{\hat{\epsilon}_k}{\|u_{k-1} - u_{k-2}\|}\right\}, & \text{if } u_{k-1} \neq u_{k-2}, \\ \psi, & \text{otherwise} \end{cases} \tag{8}$$

Generate the inertial iterate as $\eta_k = u_k + \phi_k(u_k - u_{k-1}) + \psi_k(u_{k-1} - u_{k-2})$, and then compute $\mathfrak{F}(\eta_k)$. If $\|\mathfrak{F}(\eta_k)\| \leq \varepsilon$, the algorithm terminates.

Step 3. Consider an arbitrary CG parameter β_k and an arbitrary vector p_k. Calculate the composite search direction d_k by

$$d_k = \begin{cases} -\mathfrak{F}(\eta_k), & (k=0) \\ -\theta_k \mathfrak{F}(\eta_k) + \beta_k d_{k-1}, & (k \geq 1) \text{ if } \|\mathfrak{F}(\eta_k)\| \geq |\beta_k| \|d_{k-1}\|, \\ -\mathfrak{F}(\eta_k), & \text{if } \|p_k\| = 0 \text{ or } \|y_{k-1}\| = 0 \\ -\mathfrak{F}(\eta_k) + \frac{\mathfrak{F}(\eta_k)^\top y_{k-1}}{\varrho \|p_k\| \cdot \|y_{k-1}\|} \cdot p_k, & \text{if } \|p_k\| \neq 0 \text{ and } \|y_{k-1}\| \neq 0 \end{cases}, \ (k \geq 1) \text{ otherwise}, \tag{9}$$

where $y_{k-1} = \mathfrak{F}(\eta_k) - \mathfrak{F}(\eta_{k-1})$, θ_k is defined by

$$\theta_k = c + \beta_k \frac{\mathfrak{F}(\eta_k)^\top d_{k-1}}{\|\mathfrak{F}(\eta_k)\|^2} \tag{10}$$

If $\|d_k\| = 0$, terminate the algorithm.

Step 4. Let $z_k = \eta_k + t_k d_k$, where the step-length $t_k := \varsigma \rho^{i_k}$ and i_k is the smallest nonnegative integer i that satisfies

$$-\mathfrak{F}(\eta_k + \varsigma\rho^{i_k} d_k)^\top d_k \geq \sigma \varsigma \rho^{i_k} \frac{\|\mathfrak{F}(\eta_k + \varsigma\rho^{i_k} d_k)\|}{\mu_1 + \|\mathfrak{F}(\eta_k + \varsigma\rho^{i_k} d_k)\|} \cdot \frac{\|d_k\|^2}{\mu_2 + \|d_k\|^2} \tag{11}$$

If $\|\mathfrak{F}(z_k)\| \leq \varepsilon$, terminate the algorithm.

Step 5. Calculate$u_{k+1} = \eta_k - \gamma_k \xi_k \mathfrak{F}(z_k)$, where

$$\xi_k = \frac{\mathfrak{F}(z_k)^\top (\eta_k - z_k)}{\|\mathfrak{F}(z_k)\|^2}$$

Let $k := k + 1$, and proceed back to Step 1.

Remark 1. Different from most existing studies on CG-type projection methods for solving SoNME (1), this work, similar to [36, 37], uses three-step iterative information to generate inertial points. When the parameters are set with $\phi = \psi = 0$ and $\gamma_k \equiv 1$, rsASCGP-AF simplifies to the traditional CG-type projection method. From Step 2 of rsASCGP-AF, for any k, it is known that $\phi_k \|u_k - u_{k-1}\| \leq \epsilon_k$ and $\psi_k \|u_{k-1} - u_{k-2}\| \leq \hat{\epsilon}_k$, and

$$\sum_{k=0}^{+\infty} \phi_k \|u_k - u_{k-1}\| \leq \sum_{k=0}^{+\infty} \epsilon_k < +\infty, \quad \sum_{k=0}^{+\infty} \psi_k \|u_{k-1} - u_{k-2}\| \leq \sum_{k=0}^{+\infty} \hat{\epsilon}_k < +\infty$$

Furthermore, $\lim_{k\to+\infty} \phi_k \|u_k - u_{k-1}\| = 0$ and $\lim_{k\to+\infty} \psi_k \|u_{k-1} - u_{k-2}\| = 0$.

Remark 2. The composite search direction d_k generated by rsASCGP-AF can, in form, be interpreted as a hybrid strategy, wherein search directions are selected alternately. Nevertheless, it may also be understood as a direction that integrates a restart strategy. Within the composite direction d_k (9), we refer to

$$d_k = -\theta_k \mathfrak{F}(\eta_k) + \beta_k d_{k-1}$$

as the non-restart direction. When $k \geq 1$ and $\|\mathfrak{F}(\eta_k)\| < |\beta_k| \|d_{k-1}\|$, the restart direction is applied, defined as

$$d_k = \begin{cases} -\mathfrak{F}(\eta_k), & \text{if } \|p_k\| = 0 \text{ or } \|y_{k-1}\| = 0, \\ -\mathfrak{F}(\eta_k) + \frac{\mathfrak{F}(\eta_k)^\top y_{k-1}}{\varrho \|p_k\| \cdot \|y_{k-1}\|} \cdot p_k, & \text{if } \|p_k\| \neq 0 \text{ and } \|y_{k-1}\| \neq 0 \end{cases}$$

which is then used to compute d_k. Due to the introduction of the restart strategy, the composite search direction d_k (9) always satisfies the sufficient descent condition and trust-region property, independent of any line search and any conjugate parameter. This ensures that the proposed rsASCGP-AF achieves the desired theoretical guarantees and numerical performance.

Lemma 1. *For each $k \geq 0$, the search direction d_k produced by rsASCGP-AF, as defined by* (9) *and* (10), *always meets the sufficient descent condition*:

$$\mathfrak{F}(\eta_k)^\top d_k \le -c_1\|\mathfrak{F}(\eta_k)\|^2 \tag{12}$$

and the trust region property:

$$c_1\|\mathfrak{F}(\eta_k)\| \le \|d_k\| \le c_2\|\mathfrak{F}(\eta_k)\| \tag{13}$$

with the constants defined as $c_1 = \min\left\{c,\ 1-\frac{1}{\rho}\right\}$, $c_2 = \max\left\{c+2,\ 1+\frac{1}{\rho}\right\}$, *and* $0 < c_1 < 1 < c_2$.

Proof. For $k = 0$, the search direction is defined as $d_0 = -\mathfrak{F}(\eta_0)$, which results in $\mathfrak{F}(\eta_0)^\top d_0 = -\|\mathfrak{F}(\eta_0)\|^2$, satisfying condition (12). We now proceed to demonstrate that condition (12) holds for $k \ge 1$ through two cases.

(i-a) When $\|\mathfrak{F}(\eta_k)\| \ge |\beta_k|\|d_{k-1}\|$, considering the first case for d_k where $k \ge 1$, we derive

$$\begin{aligned}\mathfrak{F}(\eta_k)^\top d_k &= -\theta_k\|\mathfrak{F}(\eta_k)\|^2 + \beta_k\mathfrak{F}(\eta_k)^\top d_{k-1}\\ &= -\left(c + \beta_k\frac{\mathfrak{F}(\eta_k)^\top d_{k-1}}{\|\mathfrak{F}(\eta_k)\|^2}\right)\|\mathfrak{F}(\eta_k)\|^2 + \beta_k\mathfrak{F}(\eta_k)^\top d_{k-1}\\ &= -c\|\mathfrak{F}(\eta_k)\|^2\end{aligned}$$

(i-b) For the case when $\|\mathfrak{F}(\eta_k)\| < |\beta_k|\|d_{k-1}\|$, we consider the second case for d_k with $k \ge 1$. If $\|p_k\| = 0$ or $\|y_k\| = 0$, then condition (12) is trivially satisfied; otherwise, we obtain

$$\begin{aligned}\mathfrak{F}(\eta_k)^\top d_k &= -\|\mathfrak{F}(\eta_k)\|^2 + \frac{\mathfrak{F}(\eta_k)^\top y_{k-1}}{\varrho\|p_k\|\cdot\|y_{k-1}\|}\cdot\mathfrak{F}(\eta_k)^\top p_k\\ &\le -\|\mathfrak{F}(\eta_k)\|^2 + \frac{|\mathfrak{F}(\eta_k)^\top y_{k-1}|}{\varrho\|p_k\|\cdot\|y_{k-1}\|}|\mathfrak{F}(\eta_k)^\top p_k|\\ &\le -\|\mathfrak{F}(\eta_k)\|^2 + \frac{1}{\varrho}\|\mathfrak{F}(\eta_k)\|^2\\ &= -\left(1-\frac{1}{\varrho}\right)\|\mathfrak{F}(\eta_k)\|^2\end{aligned}$$

Based on the above (i-a) and (i-b), we conclude that (12) is satisfied.

Given $d_0 = -\mathfrak{F}(\eta_0)$, it is evident that $\|d_0\| = \|\mathfrak{F}(\eta_0)\|$, which confirms that (13) holds for $k = 0$. Subsequently, we establish that (13) is also valid for $k \ge 1$. Utilizing (12) together with the Cauchy–Schwarz inequality, one establishes that the first part of (13) is satisfied. We now proceed to prove that the second part of (13) holds for $k \ge 1$ by examining two cases.

(ii-a) By combining $\|\mathfrak{F}(\eta_k)\| \ge |\beta_k|\|d_{k-1}\|$ with the first case for d_k when $k \ge 1$, we have

$$\begin{aligned}\|d_k\| &= \|-\theta_k\mathfrak{F}(\eta_k) + \beta_k d_{k-1}\|\\ &\le \left(c + |\beta_k|\frac{|\mathfrak{F}(\eta_k)^\top d_{k-1}|}{\|\mathfrak{F}(\eta_k)\|^2}\right)\|\mathfrak{F}(\eta_k)\| + |\beta_k|\|d_{k-1}\|\\ &\le c\|\mathfrak{F}(\eta_k)\| + 2|\beta_k|\|d_{k-1}\|\\ &\le (c+2)\|\mathfrak{F}(\eta_k)\|\end{aligned}$$

(ii-b) From the second case for d_k when $k \ge 1$, we get

$$\begin{aligned}\|d_k\| &\le \|-\mathfrak{F}(\eta_k)\| + \left\|\frac{\mathfrak{F}(\eta_k)^\top y_{k-1}}{\varrho\|p_k\|\cdot\|y_{k-1}\|}\cdot p_k\right\|\\ &\le \|\mathfrak{F}(\eta_k)\| + \frac{1}{\varrho}\|\mathfrak{F}(\eta_k)\|\\ &\le \left(1+\frac{1}{\varrho}\right)\|\mathfrak{F}(\eta_k)\|\end{aligned}$$

This completes the proof that (13) holds for all $k \ge 1$. □

Lemma 2. *Suppose that the sequences* $\{\mathfrak{F}(\eta_k)\}$ *and* $\{d_k\}$ *are yielded by rsASCGP-AF. Then the line search* (11) *is well-defined, which means that for each* $k \ge 0$, *there exists a nonnegative integer* i_k *such that* (11) *holds.*

Proof. Assume by contradiction that there exists $k_0 \ge 0$ such that (11) fails for all nonnegative integers i, that is,

$$-\mathfrak{F}(\eta_{k_0} + \varsigma\rho^i d_{k_0})^\top d_{k_0} < \sigma\varsigma\rho^i\frac{\|\mathfrak{F}(\eta_{k_0} + \varsigma\rho^i d_{k_0})\|}{\mu_1 + \|\mathfrak{F}(\eta_{k_0} + \varsigma\rho^i d_{k_0})\|}\cdot\frac{\|d_{k_0}\|^2}{\mu_2 + \|d_{k_0}\|^2}$$

As we take the limit as $i \to +\infty$ in the above inequality, and considering the continuity of $\mathfrak{F}$ along with the fact that $\rho \in (0,1)$, we find that $\mathfrak{F}(\eta_{k_0})^\top d_{k_0} \ge 0$, which contradicts $\mathfrak{F}(\eta_{k_0})^\top d_{k_0} \le -c_1\|\mathfrak{F}(\eta_{k_0})\|^2 < 0$. Thus, the line search (11) is well-defined, and the proof is complete. □

3 | Theoretical Convergence

In this subsection, we demonstrate the global convergence of the proposed method. For the subsequent analysis, we assume that the sequences $\{u_k\}$, $\{\eta_k\}$, and $\{z_k\}$ are generated by the proposed rsASCG-AF. Additionally, the following Assumption 1 is necessary.

Assumption 1.

i. The solution set $Sol_{\mathfrak{F}}$ of SoNME (1) is nonempty.

ii. The mapping $\mathfrak{F}(\cdot)$ is continuous and monotone on $\mathbb{R}^n$.

Lemma 3 ([48]). *For the nonnegative sequences of real numbers* $\{a_k\}$ *and* $\{b_k\}$, *which meet* $a_{k+1} \le a_k + b_k$, *if* $\sum_{k=1}^{+\infty} b_k < +\infty$, *then* $\{a_k\}$ *is convergent.*

Lemma 4. *Let* $u^* \in Sol_{\mathfrak{F}}$ *be an arbitrary solution of SoNME* (1). *Assuming Assumption 1 is valid, the sequence* $\{\|u_k - u^*\|\}$ *is convergent.*

Proof. According to $z_k = \eta_k + t_k d_k$ and the line search (11), we have

$$\begin{aligned}\mathfrak{F}(z_k)^\top(\eta_k - z_k) = -t_k\mathfrak{F}(z_k)^\top d_k &\ge \sigma\frac{\|\mathfrak{F}(z_k)\|}{\mu_1 + \|\mathfrak{F}(z_k)\|}\cdot\frac{t_k^2\|d_k\|^2}{\mu_2 + \|d_k\|^2}\\ &= \sigma\frac{\|\mathfrak{F}(z_k)\|}{\mu_1 + \|\mathfrak{F}(z_k)\|}\cdot\frac{\|\eta_k - z_k\|^2}{\mu_2 + \|d_k\|^2} > 0\end{aligned}$$

This, combined with Assumption 1(ii) and $u^* \in Sol_{\mathfrak{F}}$, implies that

$$\begin{aligned}\mathfrak{F}(z_k)^\top(\eta_k-u^*) &= \mathfrak{F}(z_k)^\top(\eta_k-z_k)+\mathfrak{F}(z_k)^\top(z_k-u^*)\\ &= \mathfrak{F}(z_k)^\top(\eta_k-z_k)+[\mathfrak{F}(z_k)-\mathfrak{F}(u^*)]^\top(z_k-u^*)\\ &\geq \mathfrak{F}(z_k)^\top(\eta_k-z_k)\\ &\geq \sigma\frac{\|\mathfrak{F}(z_k)\|}{\mu_1+\|\mathfrak{F}(z_k)\|}\cdot\frac{\|\eta_k-z_k\|^2}{\mu_2+\|d_k\|^2} > 0 \end{aligned} \tag{14}$$

where the first inequality is derived via the monotonicity of $\mathfrak{F}(\cdot)$. Further utilizing Step 5 of Algorithm 1, we obtain

$$\begin{aligned}&\|u_{k+1}-u^*\|^2\\ &= \|\eta_k-\gamma_k\xi_k\mathfrak{F}(z_k)-u^*\|^2\\ &= \|\eta_k-u^*\|^2-2\gamma_k\xi_k\mathfrak{F}(z_k)^\top(\eta_k-u^*)+\gamma_k^2\xi_k^2\|\mathfrak{F}(z_k)\|^2\\ &\leq \|\eta_k-u^*\|^2-2\gamma_k\xi_k\mathfrak{F}(z_k)^\top(\eta_k-z_k)+\gamma_k^2\xi_k^2\|\mathfrak{F}(z_k)\|^2\\ &= \|\eta_k-u^*\|^2-\gamma_k(2-\gamma_k)\frac{[\mathfrak{F}(z_k)^\top(\eta_k-z_k)]^2}{\|\mathfrak{F}(z_k)\|^2}\\ &\leq \|\eta_k-u^*\|^2-\gamma_k(2-\gamma_k)\frac{\sigma^2\|\eta_k-z_k\|^4}{(\mu_1+\|\mathfrak{F}(z_k)\|)^2(\mu_2+\|d_k\|^2)^2}\\ &\leq \|\eta_k-u^*\|^2-\underline{\gamma}(2-\overline{\gamma})\frac{\sigma^2\|\eta_k-z_k\|^4}{(\mu_1+\|\mathfrak{F}(z_k)\|)^2(\mu_2+\|d_k\|^2)^2} \end{aligned} \tag{15}$$

where the first inequality is obtained by (14). Furthermore, based on $0 < \underline{\gamma} \leq \overline{\gamma} < 2$ and Remark 1, one has

$$\begin{aligned}\|u_{k+1}-u^*\| &\leq \|\eta_k-u^*\|\\ &= \|u_k+\phi_k(u_k-u_{k-1})+\psi_k(u_{k-1}-u_{k-2})-u^*\|\\ &\leq \|u_k-u^*\|+\phi_k\|u_k-u_{k-1}\|+\psi_k\|u_{k-1}-u_{k-2}\|\\ &\leq \|u_k-u^*\|+\epsilon_k+\hat{\epsilon}_k\end{aligned}$$

Combining Lemma 3, we know that the sequence $\{\|u_k-u^*\|\}$ converges. □

Lemma 5. *Given that Assumption 1 is met, the ensuing two conclusions can be drawn.*

(i) $\{u_k\}$, $\{\eta_k\}$, $\{d_k\}$, *and* $\{z_k\}$ *are bounded.*

(ii) $\lim_{k\to+\infty}\|\eta_k-z_k\| = \lim_{k\to+\infty}t_k\|d_k\| = 0$.

Proof. (i) By Lemma 4, we know that $\{\|u_k-u^*\|\}$ converges, and hence $\{\|u_k-u^*\|\}$ is bounded. Since $u^*\in Sol_{\mathfrak{F}}$, $\{u_k\}$ is also bounded. Therefore, there exist positive numbers N_1 and N_2 such that

$$\|u_k-u^*\|\leq N_1,\ \|u_k\|\leq N_2,\ \forall\ k\geq 0$$

Combining the definitions of ϕ_k and ψ_k, we have

$$\begin{aligned}\|\eta_k\| &= \|u_k+\phi_k(u_k-u_{k-1})+\psi_k(u_{k-1}-u_{k-2})\|\\ &\leq \|u_k\|+\phi_k\|u_k-u_{k-1}\|+\psi_k\|u_{k-1}-u_{k-2}\|\\ &\leq N_2+\epsilon_k+\hat{\epsilon}_k < N_2+2\end{aligned}$$

which implies that $\{\eta_k\}$ is bounded. Given the continuity of $\mathfrak{F}(\cdot)$, $\{\mathfrak{F}(\eta_k)\}$ is also bounded. Combining this with the trust region property (13), we deduce that $\{d_k\}$ is bounded, that is, for any $k\geq 0$, there exists $N_3(>0)$ such that $\|d_k\|\leq N_3$. Furthermore, using $z_k=\eta_k+t_kd_k$ and the fact that $t_k\in(0,\varsigma]$, we know that $\{z_k\}$ is also bounded.

(ii) Considering that $u^*\in Sol_{\mathfrak{F}}$, the definition of η_k, the Cauchy–Schwarz inequality, and Remark 1, we deduce that

$$\begin{aligned}\|\eta_k-u^*\|^2 &= \|u_k+\phi_k(u_k-u_{k-1})+\psi_k(u_{k-1}-u_{k-2})-u^*\|^2\\ &= \|u_k-u^*\|^2+2(u_k-u^*)^\top[\phi_k(u_{k-1}-u_{k-1})\\ &\quad+\psi_k(u_{k-1}-u_{k-2})]\\ &\quad+\|\phi_k(u_k-u_{k-1})+\psi_k(u_{k-1}-u_{k-2})\|^2\\ &\leq \|u_k-u^*\|^2+2\|u_k-u^*\|[\phi_k\|u_{k-1}-u_{k-1}\|\\ &\quad+\psi_k\|u_{k-1}-u_{k-2}\|]\\ &\quad+2(\phi_k\|u_k-u_{k-1}\|)^2+2(\psi_k\|u_{k-1}-u_{k-2}\|)^2\\ &\leq \|u_k-u^*\|^2+2N_1(\epsilon_k+\hat{\epsilon}_k)+2\epsilon_k^2+2\hat{\epsilon}_k^2\end{aligned} \tag{16}$$

Substituting (16) into (15), we know that

$$\begin{aligned}\|u_{k+1}-u^*\|^2 \leq \|u_k-u^*\|^2+\left[2N_1(\epsilon_k+\hat{\epsilon}_k)+2\epsilon_k^2+2\hat{\epsilon}_k^2\right]-\underline{\gamma}(2-\overline{\gamma})\\ \times\frac{\sigma^2\|\eta_k-z_k\|^4}{(\mu_1+\|\mathfrak{F}(z_k)\|)^2(\mu_2+\|d_k\|^2)^2}\end{aligned} \tag{17}$$

Furthermore, given the continuity of $\mathfrak{F}(\cdot)$ and the boundedness of $\{z_k\}$, we deduce that $\{\mathfrak{F}(z_k)\}$ is also bounded, that is, for each $k\geq 0$, there exists $N_4>0$ such that $\|\mathfrak{F}(z_k)\|\leq N_4$. Combining this with $\|d_k\|\leq N_3$, $\sum_{k=0}^{+\infty}\epsilon_k<+\infty$, and $\sum_{k=0}^{+\infty}\hat{\epsilon}_k<+\infty$, we deduce from Equation (17) that

$$\begin{aligned}&\underline{\gamma}(2-\overline{\gamma})\frac{\sigma^2}{(\mu_1+N_4)^2(\mu_2+N_3^2)^2}\sum_{k=0}^{+\infty}\|\eta_k-z_k\|^4\\ &\leq \sum_{k=0}^{+\infty}\left[\|u_k-u^*\|^2+(2N_1(\epsilon_k+\hat{\epsilon}_k)+2\epsilon_k^2+2\hat{\epsilon}_k^2)-\|u_{k+1}-u^*\|^2\right]\\ &= \|u_0-u^*\|^2-\lim_{k\to+\infty}\|u_{k+1}-u^*\|^2+\sum_{k=0}^{+\infty}(2N_1(\epsilon_k+\hat{\epsilon}_k)+2\epsilon_k^2+2\hat{\epsilon}_k^2)\\ &< +\infty\end{aligned} \tag{18}$$

which implies that $\lim_{k\to+\infty}\|\eta_k-z_k\| = \lim_{k\to+\infty}t_k\|d_k\| = 0$. This completes the proof. □

Theorem 1. *Provided that Assumption 1 is satisfied, we have* $\liminf_{k\to+\infty}\|\mathfrak{F}(\eta_k)\| = 0$. *Furthermore, it is asserted that the sequences* $\{u_k\}$, $\{\eta_k\}$, *and* $\{z_k\}$ *all converge to a solution of SoNME (1).*

Proof. We establish this theorem by the following two phases.

Phase I. Proof by contradiction. If $\liminf_{k\to+\infty}\|\mathfrak{F}(\eta_k)\| = 0$ does not hold, then there exists $\Lambda>0$ such that

$$\|\mathfrak{F}(\eta_k)\|\geq\Lambda,\ \forall\ k\geq 0$$

Furthermore, using (13), we know that for any $k\geq 0$, $\|d_k\|\geq c_1\|\mathfrak{F}(\eta_k)\|\geq c_1\Lambda>0$. Combining this with Lemma 5(ii), we have $\lim_{k\to+\infty}t_k=0$. Given the boundedness of $\{d_k\}$ and $\{\eta_k\}$ (see

Lemma 5(i) and its proof), there exist two convergent subsequences $\{d_{k_j}\}$ and $\{\eta_{k_j}\}$ such that

$$\lim_{j\to+\infty, j\in\mathcal{K}} d_{k_j} = \tilde{d}, \quad \lim_{j\to+\infty, j\in\mathcal{K}} \eta_{k_j} = \tilde{\eta}$$

where $\mathcal{K}$ is an infinite index set. It follows from Equation (12) that

$$-\mathfrak{F}(\eta_{k_j})^\top d_{k_j} \geq c_1 \|\mathfrak{F}(\eta_{k_j})\|^2, \quad \forall j \in \mathcal{K}$$

Taking the limit as $j \to +\infty$ in the above relationship and using the continuity of $\mathfrak{F}(\cdot)$, we have

$$-\mathfrak{F}(\tilde{\eta})^\top \tilde{d} \geq c_1 \|\mathfrak{F}(\tilde{\eta})\|^2 \geq c_1 \Lambda^2 > 0 \tag{19}$$

On the other hand, according to the line search (11), we know that

$$-\mathfrak{F}(\eta_{k_j} + \rho^{-1} t_{k_j} d_{k_j})^\top d_{k_j} < \sigma \rho^{-1} t_{k_j} \frac{\|\mathfrak{F}(\eta_{k_j} + \rho^{-1} t_{k_j} d_{k_j})\|}{\mu_1 + \|\mathfrak{F}(\eta_{k_j} + \rho^{-1} t_{k_j} d_{k_j})\|} \cdot \frac{\|d_{k_j}\|^2}{\mu_2 + \|d_{k_j}\|^2}$$

Similarly, letting $j \to +\infty$ in the above inequality and using the continuity of $\mathfrak{F}(\cdot)$, we obtain $-\mathfrak{F}(\tilde{\eta})^\top \tilde{d} \leq 0$. This contradicts (19). Therefore, $\liminf_{k\to+\infty} \|\mathfrak{F}(\eta_k)\| = 0$.

Phase II. Considering $\{\eta_k = u_k + \phi_k(u_k - u_{k-1}) + \psi_k(u_{k-1} - u_{k-2})\}$, the definitions of ϕ_k and ψ_k, and Remark 1, we know that

$$\begin{aligned} \|u_k - \eta_k\| &= \|u_k - (u_k + \phi_k(u_k - u_{k-1}) + \psi_k(u_{k-1} - u_{k-2}))\| \\ &\leq \phi_k \|u_k - u_{k-1}\| + \psi_k \|u_{k-1} - u_{k-2}\| \leq \epsilon_k + \hat{\epsilon}_k \end{aligned}$$

Taking the limit on both sides of the aforementioned relationship and combining $\lim_{k\to+\infty} \epsilon_k = 0$ and $\lim_{k\to+\infty} \hat{\epsilon}_k = 0$, we obtain $\lim_{k\to+\infty} \|u_k - \eta_k\| = 0$. Let

$$\lim_{j\to+\infty} \eta_{k_j} = \eta^*, \ \lim_{j\to+\infty} u_{k_j} = \eta^*, \ \lim_{j\to+\infty} \|\mathfrak{F}(\eta_{k_j})\| = \|\mathfrak{F}(\eta^*)\| = 0$$

hence $\lim_{j\to+\infty} \|\mathfrak{F}(u_{k_j})\| = \|\mathfrak{F}(\eta^*)\| = 0$. Let $u^* := \eta^* \in Sol_{\mathfrak{F}}$, using the convergence of $\{\|u_k - u^*\|\}$, we get

$$\lim_{k\to+\infty} \|u_k - u^*\| = \lim_{j\to+\infty} \|u_{k_j} - u^*\| = \lim_{j\to+\infty} \|u_{k_j} - \eta^*\| = 0$$

Thus, $\{u_k\}$ converges to $u^* \in Sol_{\mathfrak{F}}$, and $\{\eta_k\}$ also converges to u^*. Combining this with Lemma 5(ii), we know $\lim_{k\to+\infty} \|z_k - \eta_k\| = 0$, and therefore the sequence $\{z_k\}$ converges to u^* as well. This completes the proof. □

4 | Convergence-Rate Analysis

In this section, we establish both asymptotic and non-asymptotic convergence rates in terms of iteration complexity for the proposed rsASCGP-AF. To achieve this, we introduce an additional Assumption 2.

Assumption 2. The mapping $\mathfrak{F}$ is locally Lipschitz continuous on $\mathbb{R}^n$.

To simplify the description, we define $\bar{t}_k = \rho^{-1} t_k$ and $\bar{z}_k = \eta_k + \bar{t}_k d_k$. By Lemma 5(ii), it follows that $\|\bar{z}_k - \eta_k\| = \rho^{-1} t_k \|d_k\| \to 0$ as $k \to +\infty$. This, along with the convergence of $\{\eta_k\}$, implies that the sequence $\{\bar{z}_k\}$ is also convergent. Consequently, for the convergent sequences $\{\eta_k\}$, $\{z_k\}$, and $\{\bar{z}_k\}$, there exists a compact set $\Omega \subseteq \mathbb{R}^n$ such that $\{\eta_k, z_k, \bar{z}_k\} \subseteq \Omega$. Combining this with Assumption 2 and [49, Theorem 2.1.6], we conclude that there exists a constant $L > 0$ such that

$$\|\mathfrak{F}(u) - \mathfrak{F}(v)\| \leq L\|u - v\|, \quad \forall\, u, v \in \Omega \tag{20}$$

Lemma 6. *Suppose that Assumptions 1 and 2 hold. Then, for all $k \geq 0$, the step-length sequence $\{t_k\}$ satisfies*

$$t_k \geq \tilde{t} := \min\left\{\varsigma, \frac{\rho c_1 \mu_2}{(\mu_2 L + \sigma) c_2^2}\right\} > 0 \tag{21}$$

Proof. Clearly, if $t_k = \varsigma$, then (21) holds. Otherwise, $\bar{t}_k$ does not satisfy the line search (11), that is,

$$-\mathfrak{F}(\bar{z}_k)^\top d_k < \sigma \bar{t}_k \frac{\|\mathfrak{F}(\eta_k + \varsigma \rho^{i_k} d_k)\|}{\mu_1 + \|\mathfrak{F}(\eta_k + \varsigma \rho^{i_k} d_k)\|} \cdot \frac{\|d_k\|^2}{\mu_2 + \|d_k\|^2} < \frac{\sigma \bar{t}_k}{\mu_2} \|d_k\|^2$$

By combining (12) and (20), we then obtain

$$\begin{aligned} c_1 \|\mathfrak{F}(\eta_k)\|^2 &\leq -\mathfrak{F}(\eta_k)^\top d_k = (\mathfrak{F}(\bar{z}_k) - \mathfrak{F}(\eta_k))^\top d_k - \mathfrak{F}(\bar{z}_k)^\top d_k \\ &< \left(L + \frac{\sigma}{\mu_2}\right) \bar{t}_k \|d_k\|^2 = \left(L + \frac{\sigma}{\mu_2}\right) \rho^{-1} t_k \|d_k\|^2 \end{aligned}$$

Therefore, from the second inequality in Equation (13), we have

$$t_k > \frac{\rho c_1 \mu_2}{\mu_2 L + \sigma} \frac{\|\mathfrak{F}(\eta_k)\|^2}{\|d_k\|^2} > \frac{\rho c_1 \mu_2}{(\mu_2 L + \sigma) c_2^2}$$

This completes the proof. □

Theorem 2. (*Asymptotic convergence rate*) *Assuming that Assumptions 1 and 2 hold, we have*

$$\sum_{k=0}^{+\infty} \|\mathfrak{F}(\eta_k)\|^4 < +\infty \tag{22}$$

Additionally,

$$\min_{0\leq i\leq k-1} \|\mathfrak{F}(\eta_i)\|^4 = o\left(\frac{1}{k}\right) \tag{23}$$

Proof. According to (18), we know that $\sum_{k=0}^{+\infty} \|\eta_k - z_k\|^4 = \sum_{k=0}^{+\infty} t_k^4 \|d_k\|^4 < +\infty$. Moreover, it follows from the first inequality in Equation (13) that $\sum_{k=0}^{+\infty} t_k^4 \|\mathfrak{F}(\eta_k)\|^4 < +\infty$. Combining this with Lemma 6, we conclude that $\sum_{k=0}^{+\infty} \|\mathfrak{F}(\eta_k)\|^4 < +\infty$. By the Cauchy principle, we have

$$\min_{0\leq i\leq k-1} \|\mathfrak{F}(\eta_i)\|^4 = o\left(\frac{1}{k}\right) \text{ as } k \to +\infty$$

Hence, the proof is complete. □

Lemma 7. *Assuming Assumption 1 holds, for all $k \geq 1$, the following inequality holds*:

$$\tau_k + \sum_{i=0}^{k-1} \vartheta_i \leq \tau_0 + \sum_{i=0}^{k-1} \delta_i \tag{24}$$

where $\tau_k = \|u_k - u^*\|$, $\vartheta_i = \underline{\gamma}(2-\overline{\gamma})\frac{\sigma^2\|\eta_i - z_i\|^4}{(\mu_1+N_4)^2(\mu_2+N_3^2)^2}$, *and* $\delta_i = 2N_1(\epsilon_i + \hat{\epsilon}_i) + 2\epsilon_i^2 + 2\hat{\epsilon}_i^2$.

Proof. Based on (17), substituting the definitions

$$\tau_k = \|u_k - u^*\|, \quad \vartheta_k = \underline{\gamma}(2-\overline{\gamma})\frac{\sigma^2\|\eta_k - z_k\|^4}{(\mu_1+N_4)^2(\mu_2+N_3^2)^2},$$
$$\text{and} \quad \delta_k = 2N_1(\epsilon_k + \hat{\epsilon}_k) + 2\epsilon_k^2 + 2\hat{\epsilon}_k^2$$

we obtain

$$\tau_{k+1} - \tau_k + \vartheta_k \le \tau_{k+1} - \tau_k + \underline{\gamma}(2-\overline{\gamma})\frac{\sigma^2\|\eta_k - z_k\|^4}{(\mu_1+\|\mathfrak{F}(z_k)\|)^2(\mu_2+\|d_k\|^2)^2}$$
$$\le 2N_1(\epsilon_k + \hat{\epsilon}_k) + 2\epsilon_k^2 + 2\hat{\epsilon}_k^2 = \delta_k$$

As a result, by summing both sides from $i = 0$ to $k-1$, we have

$$\tau_k + \sum_{i=0}^{k-1}\vartheta_i \le \tau_0 + \sum_{i=0}^{k-1}\delta_i, \quad k \ge 1$$

The proof is thus complete. □

Theorem 3. ($O(1/k)$ *convergence rate*) *Suppose that Assumptions 1 and 2 hold. Then, there exists a constant* $s > 0$ *such that, for all* $k \ge 1$,

$$\min_{0\le i\le k-1}\|\mathfrak{F}(\eta_i)\| \le \frac{s}{\sqrt[4]{k}}$$

Proof. From the definition of δ_i, we conclude that there exists $\overline{M} > 0$ such that $\sum_{i=0}^{k-1}\delta_i = \overline{M}$ holds for any $k \ge 1$. According to (24), for every $k \ge 1$, it follows that

$$\frac{\underline{\gamma}(2-\overline{\gamma})\sigma^2 k}{(\mu_1+N_4)^2(\mu_2+N_3^2)^2}\min_{0\le i\le k-1}\|\eta_i - z_i\|^4 \le u_0 + \overline{M}$$

Combining this with the definition of z_i, we obtain

$$\frac{\underline{\gamma}(2-\overline{\gamma})\sigma^2 k}{(\mu_1+N_4)^2(\mu_2+N_3^2)^2}\min_{0\le i\le k-1}\|t_i d_i\|^4 \le u_0 + \overline{M}$$

Applying (21), we obtain

$$\min_{0\le i\le k-1}\|d_i\|^4 \le \frac{\left(u_0+\overline{M}\right)(\mu_1+N_4)^2(\mu_2+N_3^2)^2}{\underline{\gamma}(2-\overline{\gamma})\sigma^2\bar{t}^4 k}$$

Combined with the first inequality in Equation (13), this further implies that

$$\min_{0\le i\le k-1}\|\mathfrak{F}(\eta_i)\|^4 \le \frac{\left(u_0+\overline{M}\right)(\mu_1+N_4)^2(\mu_2+N_3^2)^2}{\underline{\gamma}(2-\overline{\gamma})\sigma^2\bar{t}^4 c_1^4 k}$$

Therefore, the conclusion of the theorem is established, completing the proof. □

5 | Numerical Experiments

To evaluate the effectiveness of the proposed rsASCGP-AF, we use it to solve problems involving nonlinear equations and to applications in compressed sensing. All codes are implemented on a desktop system configured with an Intel(R) Core(TM) i5-12600KF CPU at 3.7 GHz, 32 GB RAM, and running Windows 11.

5.1 | Numerical Tests on Nonlinear Equations

In this section, we evaluate the rsASCGP-AF method against five related DFP methods—ISGM2 [1], PCGA-SNE [6], MDY [7], ISTCP [24], and ISCGPM [29]—to demonstrate the numerical performance of rsASCGP-AF in solving unconstrained nonlinear equations.

For the proposed rsASCGP-AF, we set $\beta_k = \frac{\mathfrak{F}(\eta_k)(\mathfrak{F}(\eta_k)-\mathfrak{F}(\eta_{k-1}))}{\|\mathfrak{F}(\eta_{k-1})\|^2}$ and $p_k = \mathfrak{F}(\eta_k)$. The algorithm parameters are configured as follows: $\sigma = 0.0001$, $\phi = 0.001$, $\psi = 0.002$, $\rho = 3$, $c = 1$, $\varsigma = 1$, $\rho = 0.6$, $\mu_1 = 5$, $\mu_2 = 4$, $\gamma_k \equiv 1.5$, and $\epsilon_k = \hat{\epsilon}_k = \frac{1}{k^2}$ ($\epsilon_k = \hat{\epsilon}_k = 1$, if $k = 0$). For the five comparison methods, we use the parameter settings as originally defined in their respective papers. The rsASCGP-AF requires three points: u_{-2}, u_{-1}, and u_0 to generate inertial iterates. Similarly, the ISGM2, ISTCP, and ISCGPM require two initial values, u_{-1} and u_0. Conversely, the PCGA-SNE and MDY use a single initial point, u_0. We use the following Problems 1–10 with seven values for the dimension: $n = 5$, $n = 10^2$, $n = 5\times10^2$, $n = 10^3$, $n = 10^4$, 5×10^4, and 10^5, respectively. Table 1 lists 7 different initial points.

Let $\mathfrak{F}(u) = \left(\mathfrak{f}_1(u), \mathfrak{f}_2(u), \ldots, \mathfrak{f}_n(u)\right)^\top$. The list below presents 10 tested problems.

Problem 1 ([1]). Set

$$\mathfrak{f}_1(u) = u_1 + \sin(u_1) - 1,$$
$$\mathfrak{f}_i(u) = -u_{i-1} + 2u_i + \sin(u_i) - 1, \text{ for } i = 2, 3, \ldots, n-1,$$
$$\mathfrak{f}_n(u) = u_n + \sin(u_n) - 1$$

Problem 2 ([2]). Set $\mathfrak{f}_i(u) = e^{u_i} + 1.5\sin(2u_i) - 1$, for $i = 1, 2, \ldots, n$.

Problem 3 ([6]). Set $\mathfrak{f}_i(u) = u_i - \sin(|u_i - 1|)$, for $i = 1, 2, 3, \ldots, n$.

TABLE 1 | Initial points.

Case	u_{-2}	u_{-1}	u_0
I	$(0.1, 0.1, \ldots, 0.1)^\top$	$(0.2, 0.2, \ldots, 0.2)^\top$	$(0.1, 0.1, \ldots, 0.1)^\top$
II	$(0.2, 0.2, \ldots, 0.2)^\top$	$(0.1, 0.1, \ldots, 0.1)^\top$	$(0.2, 0.2, \ldots, 0.2)^\top$
III	$(0.2, 0.2, \ldots, 0.2)^\top$	$(0.1, 0.1, \ldots, 0.1)^\top$	$(0.5, 0.5, \ldots, 0.5)^\top$
IV	$(0.2, 0.2, \ldots, 0.2)^\top$	$(0.1, 0.1, \ldots, 0.1)^\top$	$(1.2, 1.2, \ldots, 1.2)^\top$
V	$(0.2, 0.2, \ldots, 0.2)^\top$	$(0.1, 0.1, \ldots, 0.1)^\top$	$(1.5, 1.5, \ldots, 1.5)^\top$
VI	$(0.2, 0.2, \ldots, 0.2)^\top$	$(0.1, 0.1, \ldots, 0.1)^\top$	$(2, 2, \ldots, 2)^\top$
VII	$(0.2, 0.2, \ldots, 0.2)^\top$	$(0.1, 0.1, \ldots, 0.1)^\top$	rand$(n, 1)$

Problem 4 ([7]). Set $\mathfrak{f}_i(u) = 2u_i - \sin(|u_i|)$, for $i = 1, 2, 3, \ldots, n$.

Problem 5 ([8]). Set

$$\begin{aligned}
\mathfrak{f}_1(u) &= 4u_1 - u_2 + e^{u_1} - 5,\\
\mathfrak{f}_i(u) &= 4u_i - u_{i-1} - u_{i+1} + e^{u_i} - 5, \text{ for } i = 2, 3, \ldots, n-1,\\
\mathfrak{f}_n(u) &= 4u_n - u_{n-1} + e^{u_n} - 5
\end{aligned}$$

Problem 6 ([9]). Set $\mathfrak{f}_i(u) = \cos(u_i) + u_i - 1$, for $i = 1, 2, 3, \ldots, n$.

Problem 7 ([16]). Set

$$\begin{aligned}
\mathfrak{f}_1(u) &= 3u_1^3 + 2u_2 - 5 + \sin(u_1 - u_2)\sin(u_1 + u_2),\\
\mathfrak{f}_i(u) &= -u_{i-1}e^{u_{i-1}-u_i} + u_i(4 + 3u_i^2) + 2u_{i+1}\\
&\quad + \sin(u_i - u_{i+1})\sin(u_i + u_{i+1}) - 8, \text{ for } i = 2, 3, \ldots, n-1,\\
\mathfrak{f}_n(u) &= -u_{n-1}e^{u_{n-1}-u_n} + 4u_n - 3
\end{aligned}$$

Problem 8 ([19]). Set $\mathfrak{f}_i(u) = \sqrt{8}u_i - 1$, for $i = 1, 2, \ldots, n$.

Problem 9 ([21]). Set $\mathfrak{f}_1(u) = e^{u_1} - 1, \mathfrak{f}_i(u) = e^{u_i} + u_i - 1$, for $i = 2, \ldots, n$.

Problem 10 ([28]). Set $\mathfrak{f}_i(u) = \ln(u_i + 1) - \frac{u_i}{n}$, for $i = 1, 2, \ldots, n$.

When one of the following conditions is met, the iterative testing of the methods is terminated: (i) $\|d_k\| \le 10^{-6}$, (ii) $\|\mathfrak{F}_k\| \le 10^{-6}$, (iii) Itr ≥ 2000, where $\mathfrak{F}_k$ denotes $\mathfrak{F}(u_k)$, $\mathfrak{F}(\eta_k)$, or $\mathfrak{F}(z_k)$, and "Itr" represents the iteration count. The comparative outcomes are available at the provided online source https://www.cnblogs.com/LLHA0/p/18353934. In Table 1, the "Case" column outlines seven initial points, "n" indicates the problem dimension, "NF" refers to the number of function evaluations, "Time" represents the computational time, and "$\|\mathfrak{F}^*\|$" is the final norm of $\|\mathfrak{F}_k\|$ when the procedure is terminated. Additionally, if a method fails to find a solution, the values for "Itr/NF/Time/$\|\mathfrak{F}^*\|$" should all be recorded as "NaN".

To provide a more intuitive presentation of the numerical results for the compared methods, we use performance profiles introduced by Dolan and Moré [50] to demonstrate the computational efficiency across different methods. Generally speaking, a higher curve on the profile indicates a method with better numerical performance. Moreover, the corresponding experimental results are illustrated in Figures 1–3.

Based on the above numerical experiments, we conclude that rsASCGP-AF demonstrates superior performance in solving all test problems, achieving better results in terms of Itr, NF, and Time. Although the ISTCP method also successfully solves all test problems, its numerical performance is generally inferior to that of rsASCGP-AF. In contrast, the other four methods—ISGM2, PCGA-SNE, MDY, and ISCGPM—exhibit limitations in solving certain problems and show inferior numerical results compared to rsASCGP-AF. These comprehensive comparisons confirm that rsASCGP-AF outperforms ISGM2, PCGA-SNE, MDY, ISTCP, and ISCGPM, establishing the effectiveness and competitiveness of rsASCGP-AF in the given numerical experiments.

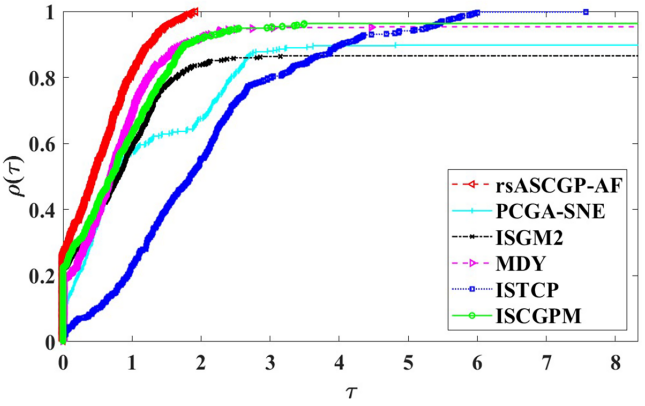

FIGURE 1 | Performance profiles of Time.

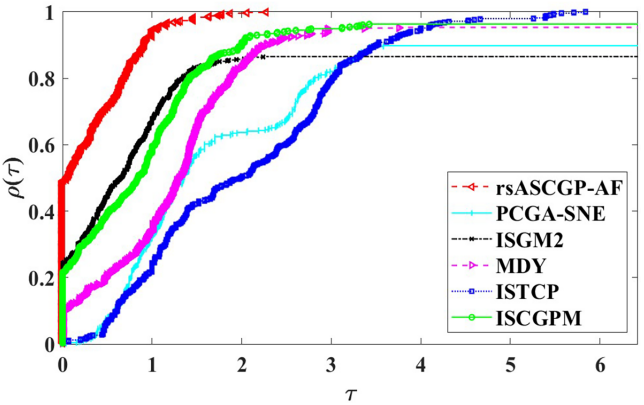

FIGURE 2 | Performance profiles of NF.

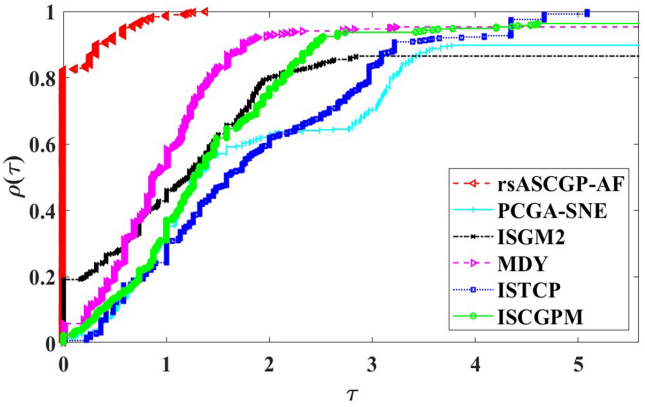

FIGURE 3 | Performance profiles of Itr.

5.2 | Applications in Compressed Sensing

In the experiment on compressed sensing, we compare rsASCGP-AF with existing methods, ISTCP [24] and ISCGPM [29]. For rsASCGP-AF, we set $\beta_k = \frac{\mathfrak{F}(\eta_k)(\mathfrak{F}(\eta_k)-\mathfrak{F}(\eta_{k-1}))}{\|\mathfrak{F}(\eta_{k-1})\|^2}$ and $p_k = \mathfrak{F}(\eta_k) - \mathfrak{F}(\eta_{k-1})$. The associated parameters are configured as $\sigma = 0.01$, $\phi = 0.01$, $\psi = 0.02$, $\varrho = 3$, $c = 1$, $\varsigma = 0.8$, $\rho = 0.5$, $\mu_1 = 5$, $\mu_2 = 4$, $\gamma_k \equiv 1.9$, and $\epsilon_k = \hat{\epsilon}_k = \frac{1}{k^2}$ ($\epsilon_k = \hat{\epsilon}_k = 1$, if $k = 0$). The parameter settings for ISTCP and ISCGPM follow those provided in their respective original references.

TABLE 2 | Numerical test results on signal restoration.

Problem size (m, n, r)	SparM-original	rsASCGP-AF Time/Itr/SparM/MSE	ISTCP Time/Itr/SparM/MSE	ISCGPM Time/Itr/SparM/MSE
(256, 1024, 32)	0.8826	0.01/94.50/0.8859/7.89e-06	0.04/233.75/0.8850/1.69e-06	0.07/318.25/0.8858/7.61e-06
(384, 1536, 48)	0.8806	0.04/110.75/0.8732/5.52e-06	0.15/229.75/0.8725/5.45e-06	0.20/342.25/0.8730/5.54e-06
(512, 2048, 64)	0.8756	0.04/93.75/0.8775/8.66e-06	0.21/220.25/0.8767/5.10e-06	0.37/305.50/0.8774/8.60e-06
(640, 2560, 80)	0.8753	0.13/92.75/0.8764/6.27e-06	0.37/222.00/0.8755/3.85e-06	0.68/356.50/0.8763/6.22e-06
(768, 3072, 96)	0.8811	0.17/90.25/0.8775/6.92e-06	0.58/211.50/0.8766/4.22e-06	0.77/297.75/0.8774/6.80e-06
(896, 3584, 112)	0.8752	0.32/86.75/0.8776/1.14e-05	1.22/230.50/0.8771/4.79e-06	1.47/293.25/0.8774/1.12e-05
(1024, 4096, 128)	0.8750	0.66/87.25/0.8739/1.00e-05	1.90/224.00/0.8736/3.87e-06	2.62/299.75/0.8738/1.00e-05

5.2.1 | Problem Description

At the core of compressed sensing is a mathematical framework designed to precisely reconstruct a signal encoded within an n-dimensional vector from just m ($m < n$) observations. This entails identifying the solution to a set of underdetermined linear equations described by $Ax = b$. To achieve this objective, a prevalent strategy is to solve an optimization problem that incorporates ℓ_1-norm regularization:

$$\min_{x\in\mathbb{R}^n} \mathfrak{f}(x) := \frac{1}{2}\|Ax - b\|^2 + \varphi\|x\|_1 \tag{25}$$

where $\|\cdot\|_1$ is the ℓ_1-regularization norm and $\varphi > 0$ is a constant to balance data fitting and sparsity.

Figueiredo et al. [51] tackled the non-smoothness of (25) by introducing a reformulation that transformed it into a bound-constrained quadratic program. For each vector $x \in \mathbb{R}^n$, two auxiliary vectors x^+ and $x^- \in \mathbb{R}^n$ are introduced to decompose x into two parts: $x = x^+ - x^-$, where $x^+ = \max\{x_i, 0\}$ and $x^- = \max\{-x_i, 0\}$ for all $i = 1, 2, \ldots, n$. Consequently, $\|x\|_1 = e_n^\top x^+ + e_n^\top x^-$, where $e_n^\top = (1, 1, \ldots, 1) \in \mathbb{R}^n$. Using this formulation, (25) can be rephrased as a convex quadratic programming problem:

$$\min_{x^+,x^-} \varphi e_n^\top x^+ + \varphi e_n^\top x^- + \frac{1}{2}\|A(x^+ - x^-) - b\|_2^2 \tag{26}$$

To proceed, (26) can be reformulated as a quadratic optimization problem:

$$\min_u \frac{1}{2}u^\top Hu + c^\top u \tag{27}$$

where

$$u = \begin{bmatrix} x^+ \\ x^- \end{bmatrix}, \quad c = \begin{bmatrix} \varphi e_n - A^\top b \\ \varphi e_n + A^\top b \end{bmatrix}, \quad H = \begin{bmatrix} A^\top A & -A^\top A \\ -A^\top A & A^\top A \end{bmatrix}$$

and H is semipositive definite.

Utilizing the optimality conditions, it is deduced that for u to be the minimal solution of (27), u fulfill

$$\mathfrak{F}(u) = \min\{u, Hu + c\} = 0$$

From [52, Lemma 2.2], we know that $\mathfrak{F} : \mathbb{R}^{2n} \to \mathbb{R}^{2n}$ is monotone.

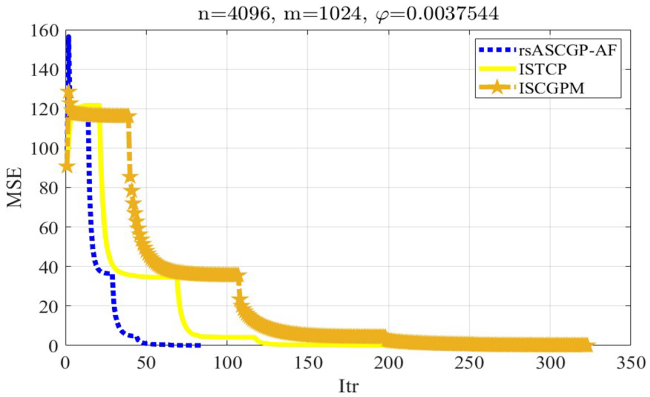

FIGURE 4 | The trend of MSE with respect to Itr.

5.2.2 | Numerical Reports

5.2.2.1 | Signal Restoration Problems. In the first numerical experiment, the matrix A is randomly generated in MATLAB, and the observed data are represented by $b = Ax + e$, where e follows a Gaussian noise distribution $N(0, \sigma^2 I)$ with $\sigma^2 = 2$. The value of φ follows Reference [51] for the tested methods, and the initial point is set as $x_0 = A^\top b$. The numerical tests are terminated when

$$\frac{|\mathfrak{f}(x_k) - \mathfrak{f}(x_{k-1})|}{|\mathfrak{f}(x_{k-1})|} < 10^{-5}$$

We then employ the sparseness measure (SparM) [53] of the observed signal, defined as

$$\text{SparM}(x) = \frac{\sqrt{n} - (\sum |x_i|)/\sqrt{x_i^2}}{\sqrt{n} - 1}$$

The quality of recovery is measured by the mean squared error (MSE):

$$\text{MSE} = \frac{1}{n}\|x^* - x\|^2$$

where x^* denotes the restored signal and x is the original signal. Generally, a lower MSE value indicates higher recovery quality for a given method.

We set $(m, n, r) = (256i, 1024i, 32i)$ with $i = 1 : 0.5 : 4$ to generate sparse signals. For each $i = 1 : 0.5 : 4$, we perform 20 random instances to evaluate performance. Table 2 presents the detailed

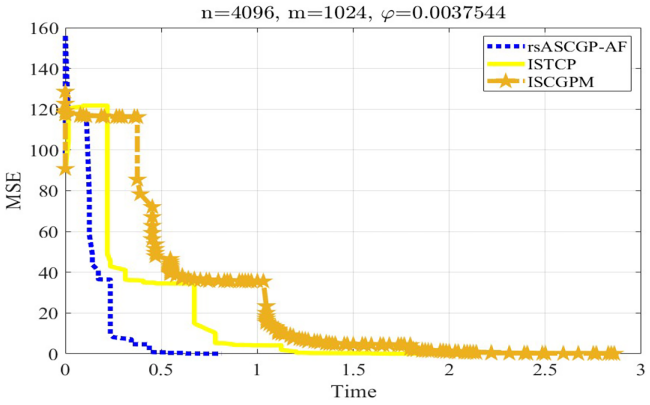

FIGURE 5 | The trend of MSE with respect to Time.

numerical results, including the sparseness of the original signal (SparM-original), the average computational time ($\overline{\text{Time}}$), the average number of iterations ($\overline{\text{Itr}}$), the average sparseness of the restored signals ($\overline{\text{SparM}}$), and the average mean squared error ($\overline{\text{MSE}}$). According to the numerical results, all three methods exhibit good performance in terms of $\overline{\text{SparM}}$ and $\overline{\text{MSE}}$, while rsASCGP-AF shows more competitive performance in $\overline{\text{Time}}$ and $\overline{\text{Itr}}$.

Under the setting $(m, n, r) = (1024, 4096, 128)$, Figures 4 and 5 illustrate the variation of MSE with respect to iterations and time, respectively, during the signal recovery process. In general, lower curves correspond to better numerical performance. Figure 6 shows the original signal, the observed signal, and the signals reconstructed by the three evaluated methods under the setting $(m, n, r) = (1024, 4096, 128)$.

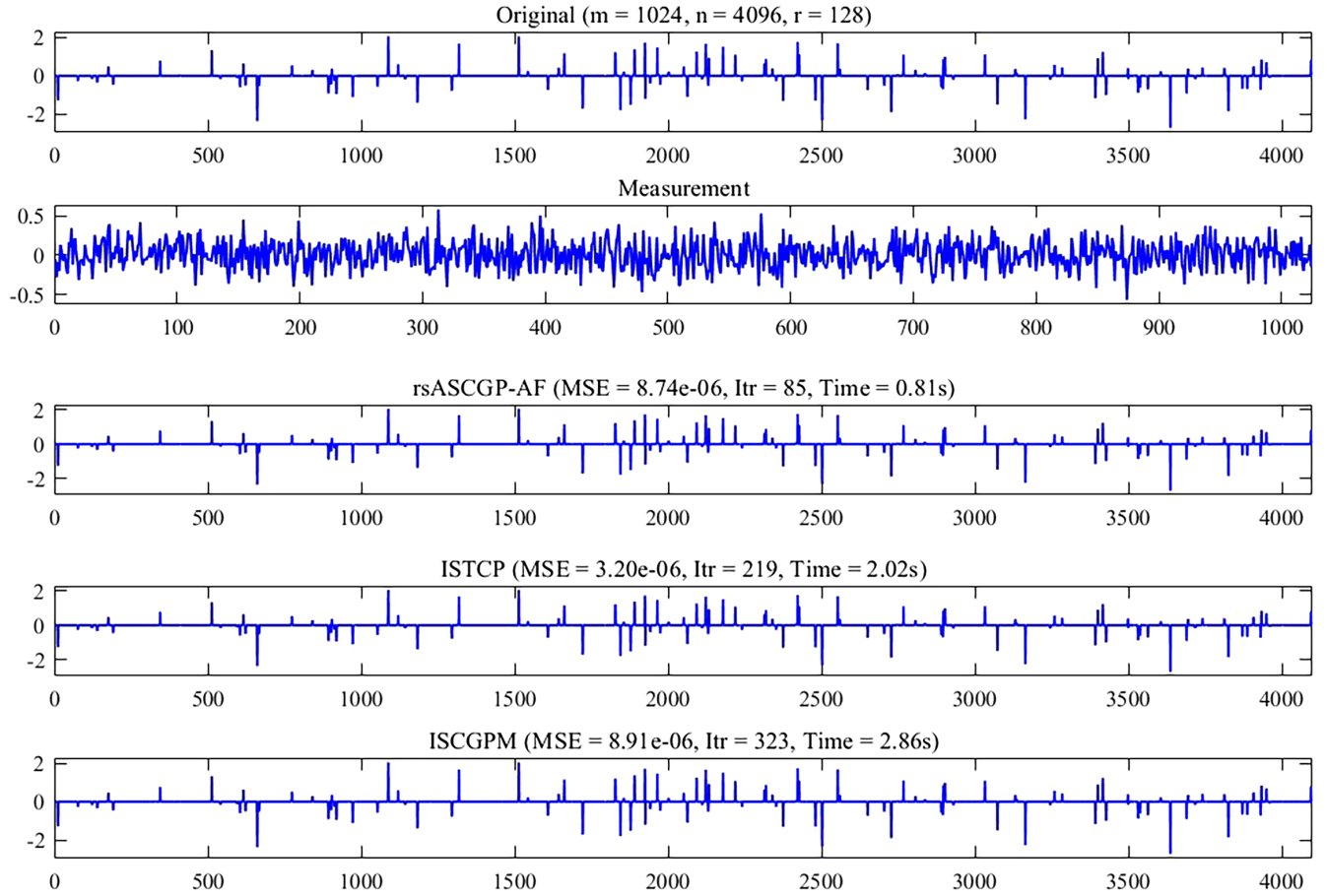

FIGURE 6 | From top to bottom: The original signal, the measurement, and the recovered signals by three tested methods.

TABLE 3 | Numerical test results on image deblurring.

Image	rsASCGP-AF	ISTCP	ISCGPM
	Itr/Time/PSNR/SSIM	Itr/Time/PSNR/SSIM	Itr/Time/PSNR/SSIM
Baboon.bmp (256 × 256)	**341**/**1.94**/**20.47**/0.50	440/3.08/20.46/0.50	594/3.66/20.44/0.50
Chart.tiff (256 × 256)	**524**/**5.55**/**27.74**/0.79	692/6.36/27.64/0.79	963/9.38/27.52/0.79
Cameraman.png (256 × 256)	**401**/**4.02**/**27.85**/0.48	518/4.59/27.79/0.48	712/5.70/27.78/0.48
Bridg.bmp (512 × 512)	**302**/**8.58**/**26.53**/0.68	395/11.50/26.52/0.68	564/20.70/26.51/0.68

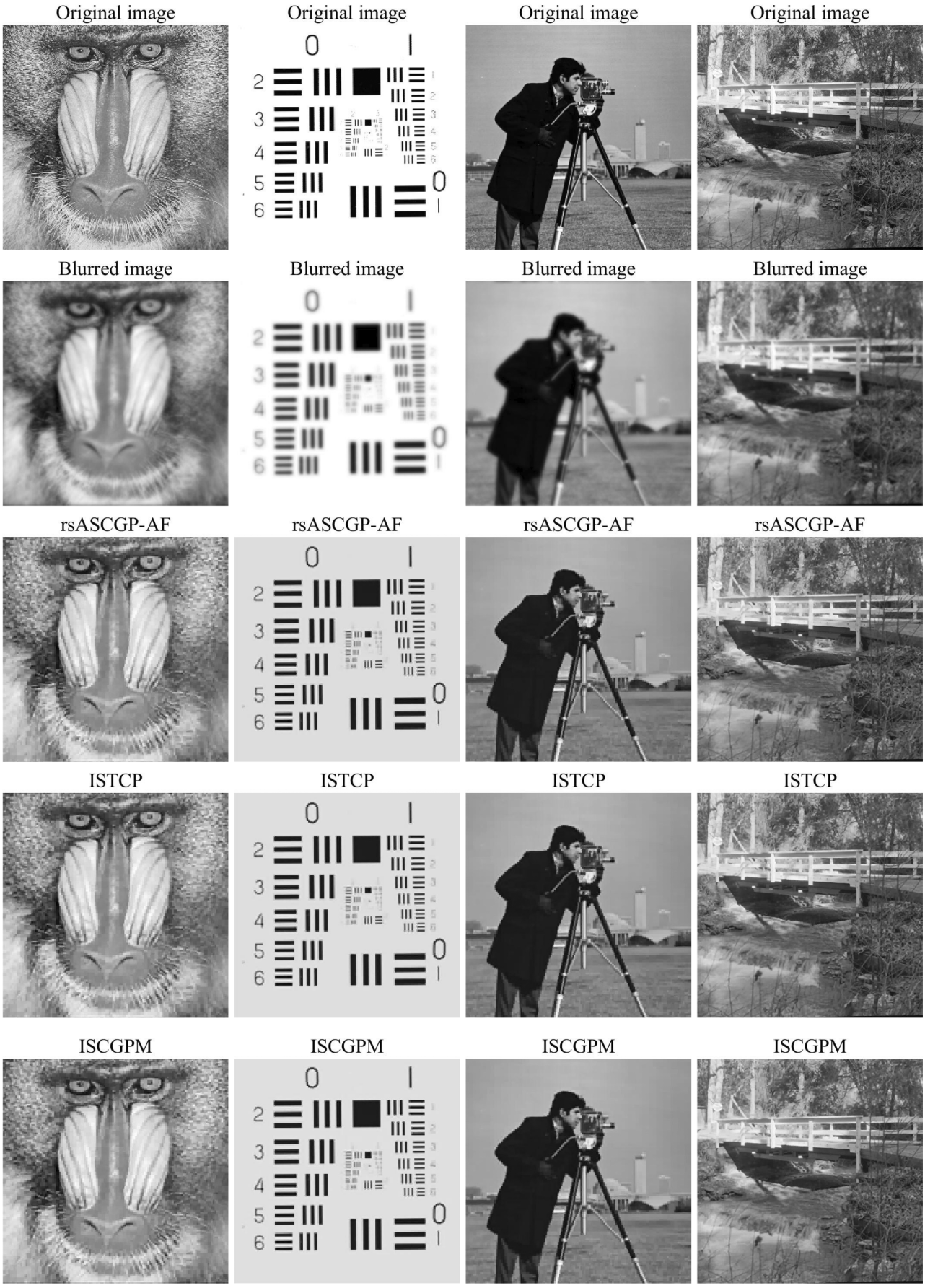

FIGURE 7 | The original images (first row), the blurred images (second row), and the deblurring images obtained by rsASCGP-AF (third row), ISTCP (fourth row), and ISCGPM (last row).

5.2.2.2 | Image Deblurring Problems. For image deblurring problems, we use two metrics—peak signal-to-noise ratio (PSNR) [54] and structural similarity index (SSIM) [55]—to quantitatively evaluate the quality of the restored images. Higher values of PSNR and SSIM indicate better image restoration quality. The numerical experiments terminate when

$$\frac{|\mathfrak{f}(x_k) - \mathfrak{f}(x_{k-1})|}{|\mathfrak{f}(x_{k-1})|} < 10^{-5}$$

The parameter values for the tested methods remain the same as in the first experiment for signal restoration problems. The images used in this study consist of a set of test images: Baboon.bmp (256 × 256), Chart.tiff (256 × 256), Cameraman.png (256 × 256), and Bridge.bmp (512 × 512). The numerical results are presented in Table 3, which reports the number of iterations (Itr), computational time (Time), PSNR, and SSIM. For each tested method, the recovered image with the highest PSNR and SSIM values indicates better restoration performance. In Table 3, we use bold font to highlight the best results for Itr, Time, and PSNR. The original, blurred, and restored images are shown in Figure 7. In summary, the numerical results demonstrate the potential of rsASCGP-AF in image deblurring problems.

6 | Conclusions

In this paper, we present an accelerated spectral CG-type projection method designed for solving the SoNME. Compared to traditional DFP methods, the proposed method employs a three-step iterative information to generate inertial iterates. The developed composite search direction incorporates an effective restart mechanism utilizing known iterative information. It satisfies both the sufficient descent condition and the trust-region property, independent of line search choices and conjugate parameters. Under conventional assumptions, we provide a rigorous proof of global convergence. When local Lipschitz continuity is assumed, we further analyze both asymptotic and non-asymptotic convergence rates in terms of iteration complexity. Numerical experiments on 10 test problems involving nonlinear equations are conducted to evaluate the performance of the proposed method. The applicability of the method is further demonstrated through preliminary experiments on signal restoration and image deblurring problems.

In addition, we note that Reference [56] establishes the conjugacy of the proposed search direction and the corresponding linear convergence rate of the method, and that Reference [57] also presents a linear convergence result for the proposed method. Although we analyze both the asymptotic and non-asymptotic convergence rates of our method in terms of iteration complexity, we must also acknowledge that, due to the structure of the proposed search direction and the limitations imposed by the line search strategy, our method does not strictly satisfy the conjugacy condition of CG methods. Moreover, it does not achieve the linear convergence rate reported in References [56, 57]. Addressing this limitation in greater depth represents a promising direction for future research.

Conflicts of Interest

The authors declare no conflicts of interest.

Data Availability Statement

The data that support the findings of this study are available from the corresponding author upon reasonable request.

References

1. S. Aji, P. Kumam, A. M. Awwal, M. M. Yahaya, and W. Kumam, "Two Hybrid Spectral Methods With Inertial Effect for Solving System of Nonlinear Monotone Equations With Application in Robotics," *IEEE Access* 9 (2021): 30918–30928.

2. S. Aji, P. Kumam, A. M. Awwal, M. M. Yahaya, and A. M. Bakoji, "A New Inertial-Based Method for Solving Pseudomonotone Operator Equations With Application," *Computational and Applied Mathematics* 42 (2023): 1.

3. J. H. Yin, J. B. Jian, and X. Z. Jiang, "A Spectral Gradient Projection Algorithm for Convex Constrained Nonsmooth Equations Based on an Adaptive Line Search," *Mathematics Numerica Sinica* Chinese 42, no. 4 (2020): 457–471.

4. A. H. Ibrahim, P. Kumam, A. B. Abubakar, and J. Abubakar, "A Derivative-Free Projection Method for Nonlinear Equations With Non-Lipschitz Operator: Application to LASSO Problem," *Mathematical Methods in the Applied Sciences* 46 (2023): 9006–9027.

5. J. H. Yin, J. B. Jian, and X. Z. Jiang, "A Generalized Hybrid CGPM-Based Algorithm for Solving Large-Scale Convex Constrained Equations With Applications to Image Restoration," *Journal of Computational and Applied Mathematics* 391 (2021): 113423.

6. W. Kumam, J. Vigo-Aguiar, and P. Kumam, "Projection Method for Solving Large-Scale System of Nonlinear Equations," *Nonlinear Convex Analysis and Optimization: An International Journal on Numerical, Computation and Applications* 2, no. 2 (2023): 93–112.

7. S. Aji, P. Kumam, A. M. Awwal, M. M. Yahaya, and K. Sitthithakerngkiet, "An Efficient DY-Type Spectral Conjugate Gradient Method for System of Nonlinear Monotone Equations With Application in Signal Recovery," *AIMS Mathematics* 6, no. 8 (2021): 8078–8106.

8. J. K. Liu, Z. L. Lu, J. L. Xu, S. Wu, and Z. W. Tu, "An Efficient Projection-Based Algorithm Without Lipschitz Continuity for Large-Scale Nonlinear Pseudo-Monotone Equations," *Journal of Computational and Applied Mathematics* 403 (2022): 113822.

9. S. B. Salihu, A. S. Halilu, M. Abdullahi, K. Ahmed, P. Mehta, and S. Murtala, "An Improved Spectral Conjugate Gradient Projection Method for Monotone Nonlinear Equations With Application," *Journal of Applied Mathematics and Computing* 70, no. 4 (2024): 3879–3915.

10. A. B. Abubakar, P. Kumam, A. H. Ibrahim, P. Chaipunya, and S. A. Rano, "New Hybrid Three-Term Spectral-Conjugate Gradient Method for Finding Solutions of Nonlinear Monotone Operator Equations With Applications," *Mathematics and Computers in Simulation* 201 (2022): 670–683.

11. P. Kumam, A. B. Abubakar, A. H. Ibrahim, H. U. Kura, B. Panyanak, and N. Pakkaranang, "Another Hybrid Approach for Solving Monotone Operator Equations and Application to Signal Processing," *Mathematical Methods in the Applied Sciences* 45 (2022): 7897–7922.

12. Z. Wan, J. Guo, J. J. Liu, and W. Y. Liu, "A Modified Spectral Conjugate Gradient Projection Method for Signal Recovery," *Signal, Image and Video Processing* 12 (2018): 1455–1462.

13. J. Guo and Z. Wan, "A Modified Spectral PRP Conjugate Gradient Projection Method for Solving Large-Scale Monotone Equations and Its Application in Compressed Sensing," *Mathematical Problems in Engineering* 2019, no. 1 (2019): 5261830.

14. J. Guo and Z. Wan, "Two Modified Single-Parameter Scaling Broyden-Fletcher-Goldfarb-Shanno Algorithms for Solving Nonlinear System of Symmetric Equations," *Symmetry* 13 (2021): 970.

15. J. H. Yin, J. B. Jian, X. Z. Jiang, M. X. Liu, and L. Z. Wang, "A Hybrid Three-Term Conjugate Gradient Projection Method for Constrained Nonlinear Monotone Equations With Applications," *Numerical Algorithms* 88 (2021): 389–418.

16. A. B. Abubakar, P. Kumam, H. Mohammad, A. H. Ibrahim, and A. I. Kiri, "A Hybrid Approach for Finding Approximate Solutions to Constrained Nonlinear Monotone Operator Equations With Applications," *Applied Numerical Mathematics* 177 (2022): 79–92.

17. P. J. Liu, H. Shao, Y. Wang, and X. Y. Wu, "A Three-Term CGPM-Based Algorithm Without Lipschitz Continuity for Constrained Nonlinear Monotone Equations With Applications," *Applied Numerical Mathematics* 175 (2022): 98–107.

18. P. J. Liu, X. Y. Wu, H. Shao, Y. Zhang, and S. H. Cao, "Three Adaptive Hybrid Derivative-Free Projection Methods for Constrained Monotone Nonlinear Equations and Their Applications," *Numerical Linear Algebra With Applications* 30, no. 2 (2023): e2471.

19. S. Aji, P. Kumam, P. Siricharoen, A. B. Abubakar, and M. M. Yahaya, "A Modified Conjugate Descent Projection Method for Monotone Nonlinear Equations and Image Restoration," *IEEE Access* 8 (2020): 158656–158665.

20. A. B. Abubakar, P. Kumam, J. K. Liu, H. Mohammad, and C. Tammer, "New Three-Term Conjugate Gradient Algorithm for Solving Monotone Nonlinear Equations and Signal Recovery Problems," *International Journal of Computer Mathematics* 100, no. 10 (2023): 1992–2013.

21. A. B. Abubakar, A. H. Ibrahim, M. Abdullahi, M. Aphane, and J. W. Chen, "A Sufficient Descent LS-PRP-BFGS-Like Method for Solving Nonlinear Monotone Equations With Application to Image Restoration," *Numerical Algorithms* 96 (2024): 1423–1464.

22. X. Z. Jiang, Z. F. Huang, and H. H. Yang, "A Conjugate Gradient Projection Method With Restart Procedure for Solving Constraint Equations and Image Restorations," *Journal of Applied Mathematics and Computing* 70 (2024): 2255–2284.

23. A. B. Abubakar, P. Kumam, H. Mohammad, A. H. Ibrahim, T. Seangwattana, and B. A. Hassan, "A Hybrid BFGS-Like Method for Monotone Operator Equations With Applications," *Journal of Computational and Applied Mathematics* 446 (2024): 115857.

24. A. H. Ibrahim, P. Kumam, M. Sun, P. Chaipunya, and A. B. Abubakar, "Projection Method With Inertial Step for Nonlinear Equations: Application to Signal Recovery," *Journal of Industrial and Management Optimization* 19, no. 1 (2022): 30–55.

25. M. V. Solodov and B. F. Svaiter, "A Globally Convergent Inexact Newton Method for Systems of Monotone Equations," in *Reformulation: Nonsmooth, Piecewise Smooth, Semismooth and Smoothing Methods*, ed. M. Fukushima and L. Qi (Kluwer Academic Publishers, 1998), 355–369.

26. B. T. Polyak, "Some Methods of Speeding Up the Convergence of Iteration Methods," *USSR Computational Mathematics and Mathematical Physics* 4, no. 5 (1964): 1–17.

27. G. D. Ma, J. C. Jin, J. B. Jian, J. H. Yin, and D. L. Han, "A Modified Inertial Three-Term Conjugate Gradient Projection Method for Constrained Nonlinear Equations With Applications in Compressed Sensing," *Numerical Algorithms* 92, no. 3 (2023): 1621–1653.

28. X. Y. Wu, H. Shao, P. J. Liu, and Y. Zhuo, "An Inertial Spectral CG Projection Method Based on the Memoryless BFGS Update," *Journal of Optimization Theory and Applications* 198 (2023): 1130–1155.

29. W. L. Liu, J. B. Jian, and J. H. Yin, "An Inertial Spectral Conjugate Gradient Projection Method for Constrained Nonlinear Pseudo-Monotone Equations," *Numerical Algorithms* 97 (2024): 985–1015.

30. P. J. Liu, H. Shao, Z. H. Yuan, X. Y. Wu, and T. L. Zheng, "A Family of Three-Term Conjugate Gradient Projection Methods With a Restart Procedure and Their Relaxed-Inertial Extensions for the Constrained Nonlinear Pseudo-Monotone Equations With Applications," *Numerical Algorithms* 94 (2023): 1055–1083.

31. J. B. Jian, Z. W. Ren, J. H. Yin, D. L. Han, and X. D. Wu, "An Effective Inertial-Relaxed CGPM for Nonlinear Monotone Equations," *Journal of Applied Mathematics and Computing* 70 (2024): 689–710.

32. X. Z. Jiang and Z. F. Huang, "An Accelerated Relaxed-Inertial Strategy Based CGP Algorithm With Restart Technique for Constrained Nonlinear Pseudo-Monotone Equations to Image de-Blurring Problems," *Journal of Computational and Applied Mathematics* 447 (2024): 115887.

33. P. J. Liu, H. Shao, Z. H. Yuan, and J. H. Zhou, "A Family of Inertial-Based Derivative-Free Projection Methods With a Correction Step for Constrained Nonlinear Equations and Their Applications," *Numerical Linear Algebra With Applications* 31, no. 2 (2024): e2533.

34. P. J. Liu, L. H. Li, H. Shao, M. X. Liu, and J. X. Fan, "An Inertial-Type CG Projection Method With Restart for Pseudo-Monotone Costs With Application to Traffic Assignment," *Networks and Spatial Economics* 25 (2025): 147–172.

35. A. H. Ibrahim, P. Kumam, A. B. Abubakar, and A. Adamu, "Accelerated Derivative-Free Method for Nonlinear Monotone Equations With an Application," *Numerical Linear Algebra With Applications* 29 (2022): e2424.

36. T. Y. Song and Z. X. Liu, "An Efficient Inertial Subspace Minimization CG Algorithm With Convergence Rate Analysis for Constrained Nonlinear Monotone Equations," *Journal of Computational and Applied Mathematics* 446 (2024): 115873.

37. A. H. Ibrahim and S. Al-Homidan, "Two-Step Inertial Derivative-Free Projection Method for Solving Nonlinear Equations With Application," *Journal of Computational and Applied Mathematics* 451 (2024): 116071.

38. C. X. Kou and Y. H. Dai, "A Modified Self-Scaling Memoryless Broyden-Fletcher-Goldfarb-Shanno Method for Unconstrained Optimization," *Journal of Optimization Theory and Applications* 165, no. 1 (2015): 209–224.

39. X. Z. Jiang, H. H. Yang, J. B. Jian, and X. D. Wu, "Two Families of Hybrid Conjugate Gradient Methods With Restart Procedures and Their Applications," *Optimization Methods and Software* 38, no. 5 (2023): 947–974.

40. X. Z. Jiang, X. M. Ye, Z. F. Huang, and M. X. Liu, "A Family of Hybrid Conjugate Gradient Method With Restart Procedure for Unconstrained Optimizations and Image Restorations," *Computers and Operations Research* 159 (2023): 106341.

41. X. Z. Jiang, L. G. Pan, M. X. Liu, and J. B. Jian, "A Family of Spectral Conjugate Gradient Methods With Strong Convergence and Its Applications in Image Restoration and Machine Learning," *Journal of the Franklin Institute* 361 (2024): 107033.

42. H. Shao, H. Guo, X. Y. Wu, and P. J. Liu, "Two Families of Self-Adjusting Spectral Hybrid DL Conjugate Gradient Methods and Applications in Image Denoising," *Applied Mathematical Modelling* 118 (2023): 393–411.

43. Z. B. Chen, H. Shao, P. J. Liu, G. X. Li, and X. L. Rong, "An Efficient Hybrid Conjugate Gradient Method With an Adaptive Strategy and Applications in Image Restoration Problems," *Applied Numerical Mathematics* 204 (2024): 362–379.

44. S. Babaie-Kafaki, N. Mirhoseini, and Z. Aminifard, "A Class of CG Algorithms Overcoming Jamming of the Iterative Solving Process and Its Application in Image Restoration," *Journal of Computational and Applied Mathematics* 442 (2024): 115727.

45. L. Zhang and W. J. Zhou, "Spectral Gradient Projection Method for Solving Nonlinear Monotone Equations," *Journal of Computational and Applied Mathematics* 196 (2006): 478–484.

46. Q. Li and D. H. Li, "A Class of Derivative-Free Methods for Large-Scale Nonlinear Monotone Equations," *IMA Journal of Numerical Analysis* 31 (2011): 1625–1635.

47. K. Amini and A. Kamandi, "A New Line Search Strategy for Finding Separating Hyperplane in Projection-Based Methods," *Numerical Algorithms* 70 (2015): 559–570.

48. B. T. Polyak, *Introduction to Optimization* (Optimization Software Inc, 1987), 49.

49. C. Ştefan, M. Radu, and N. Adriana, *Lipschitz Functions* (Springer, 2019).

50. E. D. Dolan and J. J. Moré, "Benchmarking Optimization Software With Performance Profiles," *Mathematical Programming* 91, no. 2 (2002): 201–213.

51. M. A. T. Figueiredo, R. D. Nowak, and S. J. Wright, "Gradient Projection for Sparse Reconstruction: Application to Compressed Sensing and Other Inverse Problems," *IEEE Journal of Selected Topics in Signal Processing* 1, no. 4 (2007): 586–597.

52. Y. H. Xiao, Q. Y. Wang, and Q. J. Hu, "Non-Smooth Equations Based Method for ℓ_1-Norm Problems With Applications to Compressed Sensing," *Nonlinear Analysis, Theory, Methods & Applications* 74, no. 11 (2011): 3570–3577.

53. P. O. Hoyer, "Non-Negative Matrix Factorization With Sparseness Constraints," *Journal of Machine Learning Research* 5 (2004): 1457–1469.

54. A. C. Bovik, *Handbook of Image and Video Processing* (Academic Press, 2000).

55. Z. Wang, A. C. Bovik, H. R. Sheikh, and E. P. Simoncelli, "Image Quality Assessment: From Error Visibility to Structural Similarity," *IEEE Transactions on Image Processing* 13 (2004): 600–612.

56. J. Guo and Z. Wan, "A New Three-Term Conjugate Gradient Algorithm With Modified Gradient-Differences for Solving Unconstrained Optimization Problems," *AIMS Mathematics* 8, no. 2 (2023): 2473–2488.

57. J. Guo and Z. Wan, "An Efficient Modified Residual-Based Algorithm for Large Scale Symmetric Nonlinear Equations by Approximating Successive Iterated Gradients," *Journal of Computational and Applied Mathematics* 438 (2024): 115552.